Electronic supplementary information

Edge-Segregated Ternary Pd-Pt-Ni Spiral Nanosheets as High-Performance Bifunctional Oxygen Redox Electrocatalysts for Rechargeable Zinc−Air Batteries

Kai Liu,[†a] Hongpu Huang,[†a] Yuxin Zhu,[a] Shupeng Wang,[a] Zixi Lyu,[a] Xiao Han,[b] Qin Kuang,*[b] and Shuifen Xie*[a]

[a]Xiamen Key Laboratory of Optoelectronic Materials and Advanced Manufacturing, College of Materials Science and Engineering, Huaqiao University, Xiamen 361021, China

[b]State Key Laboratory of Physical Chemistry of Solid Surfaces, Collaborative innovation center of Chemistry for Energy Materials, College of Chemistry and Chemical Engineering, Xiamen University, Xiamen 361005, China

[†]These authors contributed equally to this work.

*Corresponding Author Email: sfxie@hqu.edu.cn; qkuang@xmu.edu.cn

Experimental Section

Reagents. Hexadecyl trimethyl ammonium chloride (CTAC) was purchased from J&K Scientific; Polyvinylpyrrolidone (PVP, MW≈55000, AR) was purchased from Sigma-Aldrich; Tungsten hexacarbonyl ($W(CO)_6$, 97%) was purchased from Alfa Aesar. Platinum(II) acetylacetonate ($Pt(acac)_2$, ≥99.0%) and palladium(II) acetylacetonate ($Pd(acac)_2$, ≥99.0%) were purchased from Kunming Institute of Precious Metals. Nickel(II) acetylacetonate ($Ni(acac)_2$, ≥95.0%) was purchased from Aladdin. Iron(III) chloride ($FeCl_3$, AR, ≥99.0%) and potassium hydroxide (KOH, GR, ≥95%) were purchased from Macklin. Zinc acetate dihydrate ($C_4H_6O_4Zn.2H_2O$, AR) and acetic acid ($C_2H_4O_2$, AR) were purchased from Xilong Science Co. Ltd.. Acetone (C_3H_6O, AR, ≥99.5%) and ethanol (C_2H_5OH, AR, ≥99.7%) were obtained from Sinopharm Chemical Reagent Co. Ltd. (Shanghai, China). Ultrapure water (18.2 MΩ) was used in all the experiments. The reagents were used as obtained without further purification.

Synthesis of $Pd_{45}Pt_{44}Ni_{11}$ SpNSs. In a typical synthesis, the mixture of $Pd(acac)_2$ (8 mg), $Pt(acac)_2$ (10 mg), $Ni(acac)_2$ (8 mg), CTAC (100 mg), PVP (100 mg), $W(CO)_6$ (25 mg) and $FeCl_3$ (1.5 mg) was added together with 12.0 mL ethanol in a 25 mL Teflon autoclave, and then sealed up and stirred at 600 rpm for about 30 minutes at room temperature. The Teflon autoclave was heated from room temperature to 180 °C in around 30 min and kept at 180 °C for 1.5 hours. After cooled down to room temperature, the resulting product was collected by centrifugation (14000 rpm, 10 min) and washed with the mixture of ethanol and acetone four times, and then was re-dispersed in 2.0 mL of ethanol.

For the synthesis of monometallic Pd and bimetallic $Pd_{67}Pt_{33}$ SpNSs. For the synthesis of Pd SpNSs, $Pd(acac)_2$ (8 mg), CTAC (100 mg), PVP (100 mg), $W(CO)_6$ (25 mg) and $FeCl_3$ (1.5 mg) were mixed together with 12.0 mL of ethanol in a 25 mL Teflon autoclave. After the cap had been covered, the admixture was stirred at 600 rpm for about 30 minutes at room temperature. The Teflon autoclave was heated from room temperature to 180°C in around 30 min and retained 180°C for 1.5 hours, then cooled to room temperature. The resulting product was collected by centrifugation (14000 rpm, 10 min) and washed with ethanol/acetone four times. The washed product was re-dispersed in 2 mL of ethanol and stored. For the synthesis of PdPt SNSs, except for the addition of $Pt(acac)_2$ (10 mg), all the conditions are similar to the Pd SNS.

Characterizations. Transmission electron microscopy (TEM), high-resolution TEM (HRTEM), HAADF-STEM, EDS cross-sectional compositional line scanning profiles and elemental mappings were performed on an FEI TECNAI F30 microscope operated at 300 kV. Powder X-ray diffraction pattern (PXRD) was recorded on a Rigaku Smar/SmartLa operating at 30 mA and 40 kV using a Cu Kα radiation (λ=1.5418 Å). X-ray photoelectron spectroscopy (XPS) experiments were performed on a Thermo Scientific NEXSA (Thermo Fisher) operating at 15 mA and 15 kV using a Al Kα radiation. The XPS spectra were all corrected by C 1s peak (284.8 eV). The elemental contents of each catalyst were analyzed by ICP-MS (Agilent 7800).

Electrochemical experiments of the three-electrode system were performed on CHI 760E (Shanghai Chenhua Co., Ltd., China). UPS were recorded on the PHI5000 VersaProbe III.

Electrocatalysis Measurements. In a typical loading of before the electrocatalytic tests, the $Pd_{45}Pt_{44}Ni_{11}$ SpNSs, $Pd_{67}Pt_{33}$ SpNSs, and Pd SpNSs were loaded on Vulcan XC-72 carbon (25 wt % of PdPt total metals, measured by ICP-MS). Typically, the $Pd_{45}Pt_{44}Ni_{11}$ SpNSs, $Pd_{67}Pt_{33}$ SpNSs, and Pd SpNSs (containing 3.0 mg PdPt total metals, measured by ICP-MS) dispersed in 2 mL of ethanol and 9.0 mg Vulcan XC-72 carbon uniformly dispersed in 9 mL of ethanol were mixed under stirring treatment for 6 h to obtain the $Pd_{45}Pt_{44}Ni_{11}$ SpNSs/C, $Pd_{67}Pt_{33}$ SpNSs/C, and Pd SpNSs/C, respectively. Then, $Pd_{45}Pt_{44}Ni_{11}$ SpNSs/C, $Pd_{67}Pt_{33}$ SpNSs/C, and Pd SpNSs/C were redispersed in 5 mL of ethanol and 5 mL of acetic acid mixture, after heated at 70 °C for 10 h with magnetic stirring to clean the surface of the catalysts, respectively. The cleaned catalysts were collected by centrifugation and washed with ethanol for three times. The products were dried under vacuum condition at 50 °C for 12 h. The treated catalysts, RuO_2 and Pt/C were redispersed in the mixture containing Nafion solution and isopropanol (v:v 0.005:0.995) to form the homogeneous catalyst ink by sonicating for 20 min, respectively. The ink concentration of 0.5 $mg \cdot mL^{-1}_{Pd+Pt}$ based on ICP-MS measurement. 4 μL of the ink was transferred onto the Rotating Disk Electrode (RDE, diameter: 5 mm, area: 0.196 cm^2, Tianjin Aida Co., China) with the loading amount of PdPt at 2 μg. The loading amount of metal PdPt for the $Pd_{45}Pt_{44}Ni_{11}$ SpNSs/C, $Pd_{67}Pt_{33}$ SpNSs/C, Pd SpNSs/C, RuO_2, and Pt/C catalysts was 10 $\mu g \cdot cm^{-2}_{geo}$.

Oxygen reduction reaction (ORR) and oxygen evolution reaction (OER) measurements were conducted in 0.1 M KOH (pH = 13, O_2-saturated) solutions. All electrochemical measurements were carried out in a three-electrode system with an electrochemical workstation (CHI 760E, Shanghai Chenhua Co., China). A Pt mesh (1 × 1 cm^2) was served as counter electrodes, the saturated calomel electrode (SCE) was used as the reference electrode, and a catalyst-loaded RDE (diameter: 5 mm) was served as working electrode. All the potentials were calibrated to the RHE potential calculated from the equation $E_{RHE} = E_{SCE} + (0.241 + 0.0591\ pH)$ V, and all the potential in this letter was quoted versus RHE. For the CO stripping voltammetry measurements, the working electrode was first immersed in 0.1 M $HClO_4$ solution where CO gas (99.999%) was effervesced at a flow rate of 30 mL min^{-1} for 20 minutes. Then the pre-CO-adsorbed electrode was transferred to a saturated nitrogen 0.1 M $HClO_4$ solution. The electrochemically active surface areas (ECSAs) were determined by using the measured integrating CO stripping charges on the cyclic voltammograms (CVs) recorded between 0.05 and 1.50 V (vs. RHE) at a sweep rate of 20 mV s^{-1}. According to Equation 1:

$$ECSA = \frac{Q_{CO}}{m_{metal} \times 0.42\ mC \cdot cm - 2} \quad \text{Eq. 1}$$

The linear sweep voltammetry (LSV) of ORR was carried out between 0.2 and 1.1 V (vs. RHE). The OER polarization curves were recorded by LSV between 1.1-2.0 V (vs. RHE). The scan rate and rotation rate for ORR and OER measurements were 10 mV s^{-1} and 1600 rpm, respectively. In the accelerated durability tests (ADTs), the electrodes were performed at room temperature in 0.1 M KOH solutions (O_2-saturated) by applying the cyclic potential sweeps between 0.6 V and 1.1 V (vs. RHE) at a sweep rate of 100 mV s^{-1} for 10000 cycles.

Chronoamperometry tests were conducted in O_2-saturated 0.1 M KOH solution at a rotation rate of 1600 rpm for 12 h at 0.4 V (vs. RHE).

The kinetic current densities (j_k) and electron transfer numbers (n) per oxygen molecule in the oxygen reduction reaction were calculated by fitting the Koutecký-Levich (K-L) correlation of the above electrodes (Eq. 2, 3).

$$\frac{1}{j} = \frac{1}{j_k} + \frac{1}{j_l} \quad \text{Eq. 2}$$

$$j_l = 0.62nFD^{2/3}v^{-1/6}C\omega^{1/2} \quad \text{Eq. 3}$$

In the above equation, the j is the measured current density, j_l and j_k are the diffusion-limiting and kinetic-limiting current densities, respectively. Where F is Faraday constant (96485 C·mol^{-1}), D is the diffusion coefficient of O_2 in the 0.1 M KOH solution (1.93×10^{-5} cm^2.s^{-1}), v is the kinematic viscosity (1.01×10^{-2} cm^2·s^{-1}), and C is the concentration of O_2 in O_2-saturated 0.1M KOH solution (1.26×10^{-3} mol·L^{-1}), ω is the angular velocity of rotation ($\omega = 2\pi f$, rad·s^{-1}).

The RRDE measurement and electrode preparation methods were the same as RDE. The scanning speed of the disk electrode was 10 mV·s^{-1} and the rotation rate of 1600 rpm, the ring potential was 1.3 V. The electron transfer number (n) and the percentage of HO_2^- intermediate production (HO_2^-%) were calculated by the following equation(Eq. 4, 5).

$$n = \frac{4N * I_d}{NI_d + I_r} \quad \text{Eq. 4}$$

$$HO_2^-\% = \frac{200I_r}{NI_d + I_r} \quad \text{Eq. 5}$$

Where I_d was the disk current, I_r was ring current, and N was the current collection efficiency of the Pt ring (N = 0.37).

The Zn-air battery measurements. The liquid Zn–air battery measurements were conducted in 6 M KOH with 0.2 M $Zn(CH_3COO)_2$ was served as the electrolyte at room temperature, a polished Zn foil was served as the anode electrode. The electrocatalyst was dropped onto a carbon paper electrode (effective area 1 cm^2, Pd + Pt loading 1 mg). The waterproof and breathable layer on the other side of the carbon paper allows O_2 from ambient air to reach the catalyst, while also preventing electrolyte leakage. Squeeze the carbon paper electrode, the foamed nickel, and the waterproof and breathable membrane for 6 minutes under a pressure of 10 MPa, before it was used as the air cathode. The Zinc-air battery structures(OMS-TF1) were purchased from YOTECO(Changzhou). The polarization curves were performed on a CHI760E electrochemical workstation, and the galvanostatic charge and discharge measurements were performed on a NEWARE battery-testing system.

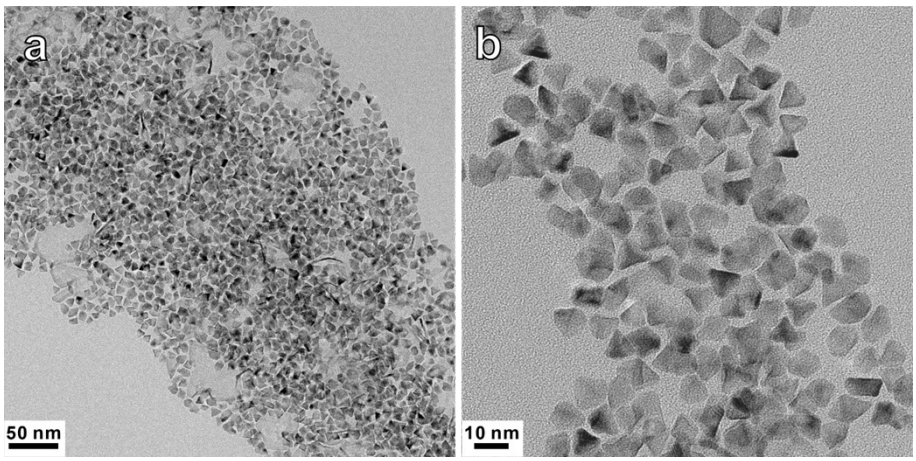

Fig. S1 TEM images of small tetrahedrons synthesized using the standard procedure without the addition of $FeCl_3$.

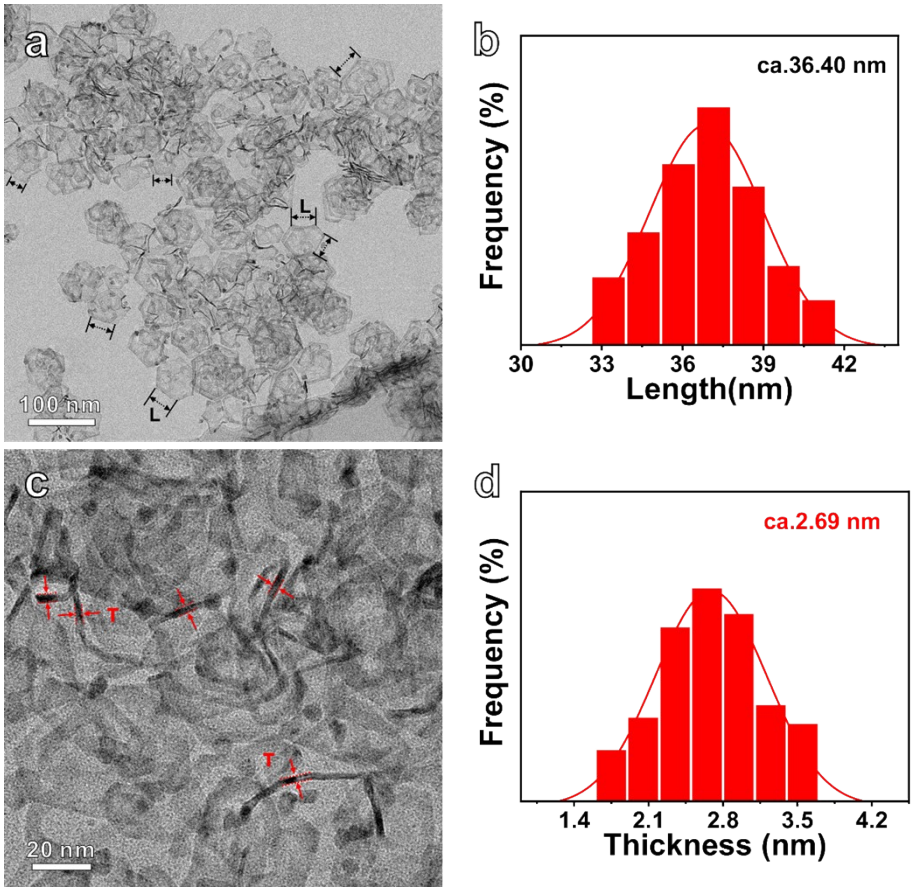

Fig. S2 Size distribution statistics of $Pd_{45}Pt_{44}Ni_{11}$ SpNSs: (a, c) TEM images; (b, d) the corresponding statistical edge length and thickness.

Table S1. Atomic ratio (determined by ICP-MS) of the products at different sampling times during synthesizing the $Pd_{45}Pt_{44}Ni_{11}$ SpNSs.

Samples	n_{Pd}(atomic %)	n_{Pt}(atomic %)	n_{Ni}(atomic %)
160 °C 0 min	96%	0%	4%
180 °C 0 min	97%	0%	3%
180 °C 5 min	97%	0%	3%
180 °C 30 min	80%	17%	3%
180 °C 90 min	45%	44%	11%

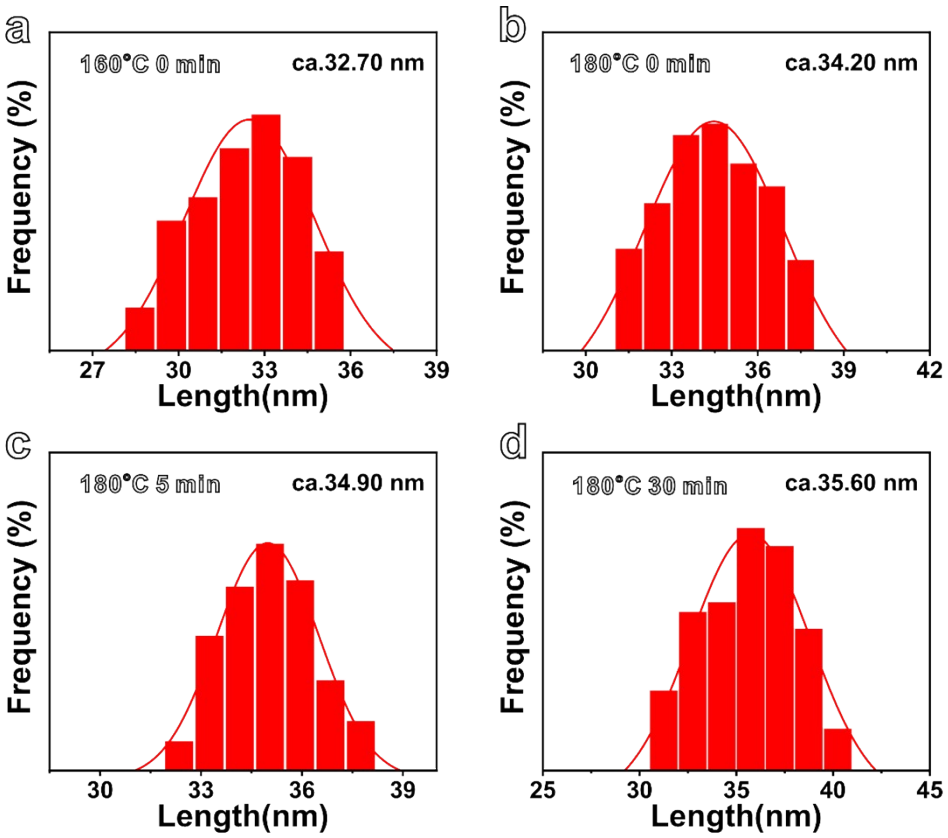

Fig. S3 Edge lengths of the samples recorded at different reaction times during synthesizing the $Pd_{45}Pt_{44}Ni_{11}$ SpNSs

Table S2. Atomic ratio of the $Pd_{45}Pt_{44}Ni_{11}$ SpNSs determined by pointwise EDS under TEM at the edge and face regions, respectively.

Edge	n_{Pd}:n_{Pt}:n_{Ni}(EDS)	**Face**	n_{Pd}:n_{Pt}:n_{Ni}(EDS)
1	30:51:19	5	80:15:5
2	34:51:15	6	64:27:9
3	30:58:12	7	64:28:8
4	34:49:17	8	77:17:6

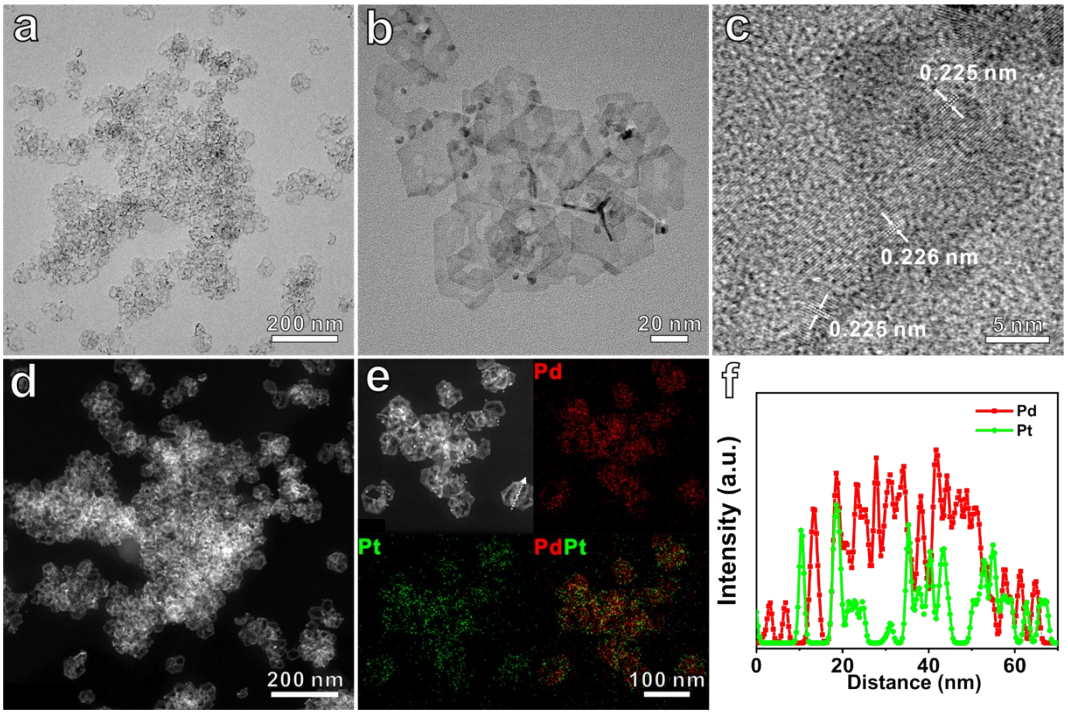

Fig. S4 Structural and elemental analysis of the $Pd_{67}Pt_{33}$ SpNSs synthesized without the addition of $Ni(acac)_2$: (a, b) TEM images; (c) HRTEM images; (d) HAADF-STEM; (e) STEM and the corresponding EDS elemental mapping; (f) EDS line scan along the white arrow marked in (e). The Pd/Pt ratio was determined by ICP-MS.

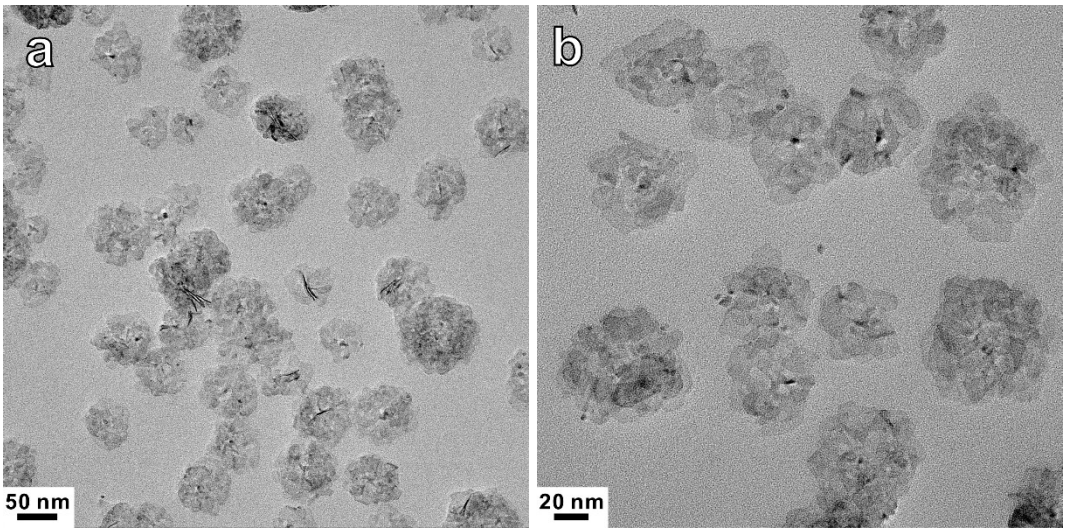

Fig. S5 TEM images of the Pd SpNSs synthesized using the standard procedure without the addition of $Pt(acac)_2$ and $Ni(acac)_2$.

Table S3. XPS analysis of the as-prepared $Pd_{45}Pt_{44}Ni_{11}$ SpNSs, $Pd_{67}Pt_{33}$ SpNSs, Pd SpNSs and commercial Pt/C and Pd/C.

Samples	**$Pd_{45}Pt_{44}Ni_{11}$ SpNSs/C**	**$Pd_{67}Pt_{33}$ SpNSs/C**	**Pd SpNSs/C**	**Pt/C**	**Pd/C**
Standard BE	71.0(Pt $4f_{7/2}$)	335.2(Pd $3d_{5/2}$)	852.6(Ni $2p_{3/2}$)	/	/
Pt $4f_{7/2}$ (eV)	70.55	70.75	/	71.65	/
Pt^0/Pt^{2+}	2.96	3.11	/	2.80	/
Pd $3d_{5/2}$ (eV)	336.00	334.90	334.70	/	336.10
Pd^0/Pd^{2+}	3.08	3.20	3.70	/	1.09
Ni $2p_{3/2}$ (eV)	852.80	/	/	/	/

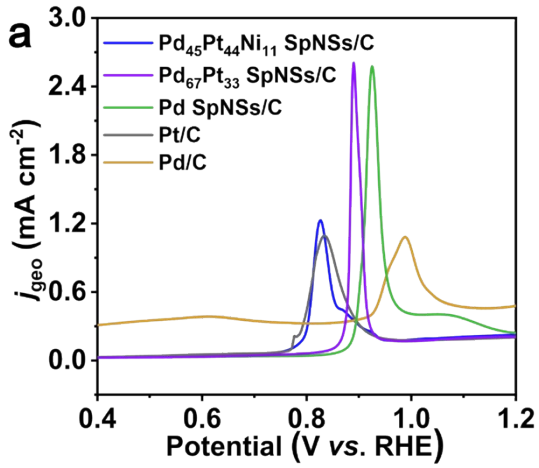

b

Samples	ECSA(m^2/g_{Pd+Pt})
$Pd_{45}Pt_{44}Ni_{11}$ SpNSs/C	82.70
$Pd_{67}Pt_{33}$ SpNSs/C	72.24
Pd SpNSs/C	92.56
Pt/C	71.50
Pd/C	45.86

Fig. S6 (a) CO stripping curves recorded in an N_2-saturated 0.1 M $HClO_4$ solution between 0.05 and 1.5 V (vs. RHE) at a sweep rate of 20 mV s^{-1} for the compared electrocatalysts and (b) The corresponding ECSA is obtained by normalizing the total Pd+Pt mass of the catalyst.

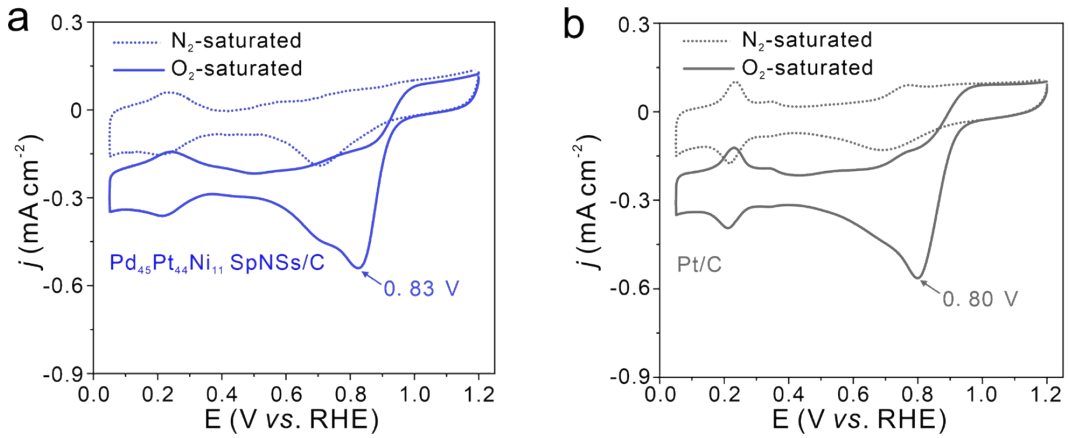

Fig. S7 (a, b) Comparative CV curves in N_2- and O_2-saturated 0.1 M KOH solution obtained from $Pd_{45}Pt_{44}Ni_{11}$ SpNSs/C and commercial Pt/C, respectively.

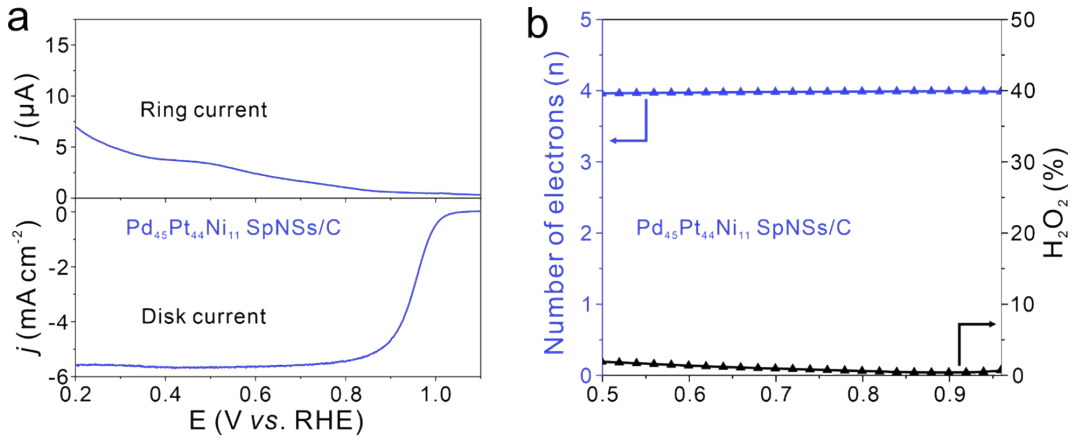

Fig. S8 (a) The RRDE measurement for the ORR selectivity of $Pd_{45}Pt_{44}Ni_{11}$ SpNSs/C in 0.1 M O_2-saturated KOH solution at 1600 rpm. (b) The corresponding transfer electron numbers and the percentage of HO_2^- according to the RRDE curves.

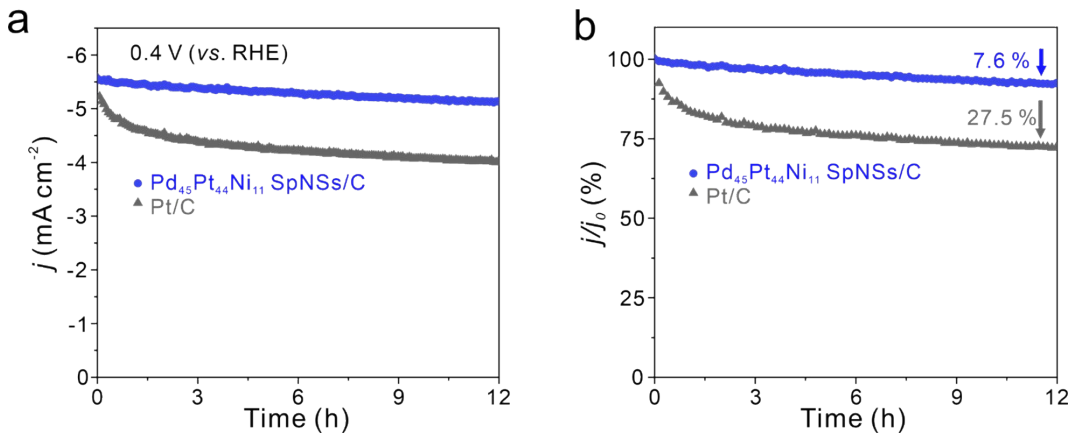

Fig. S9 (a, b) Chronoamperometry measurements for $Pd_{45}Pt_{44}Ni_{11}$ SpNSs/C and Pt/C catalysts at 0.4 V (vs. RHE) in O_2-saturated KOH solution for 12 h.

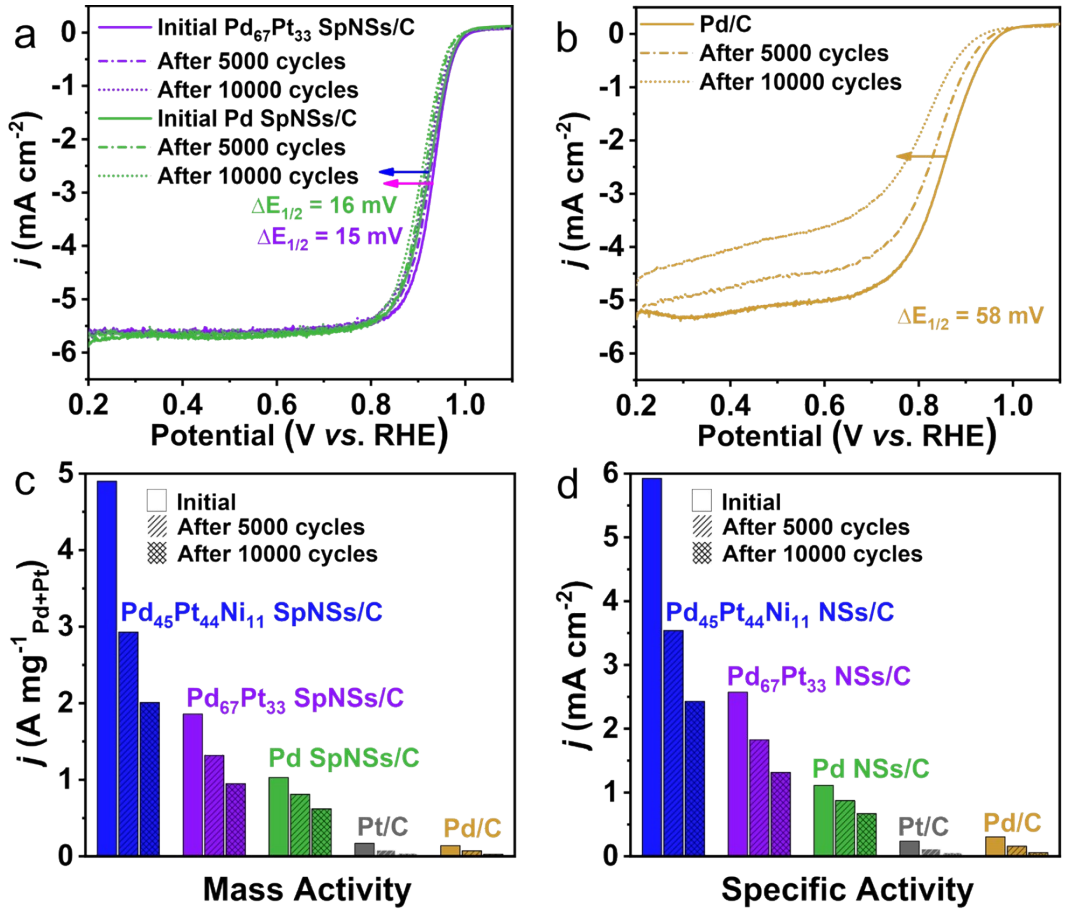

Fig. S10 ORR polarization curves before and after 5 000 and 10 000 potential cycles between 0.6 and 1.1 V versus RHE. (a, b) The $Pd_{67}Pt_{33}$ SpNSs /C, Pd SpNSs /C, Pd/C, and the commercial 20 wt% Pt/C, (c) mass activities and (d) specific activities.

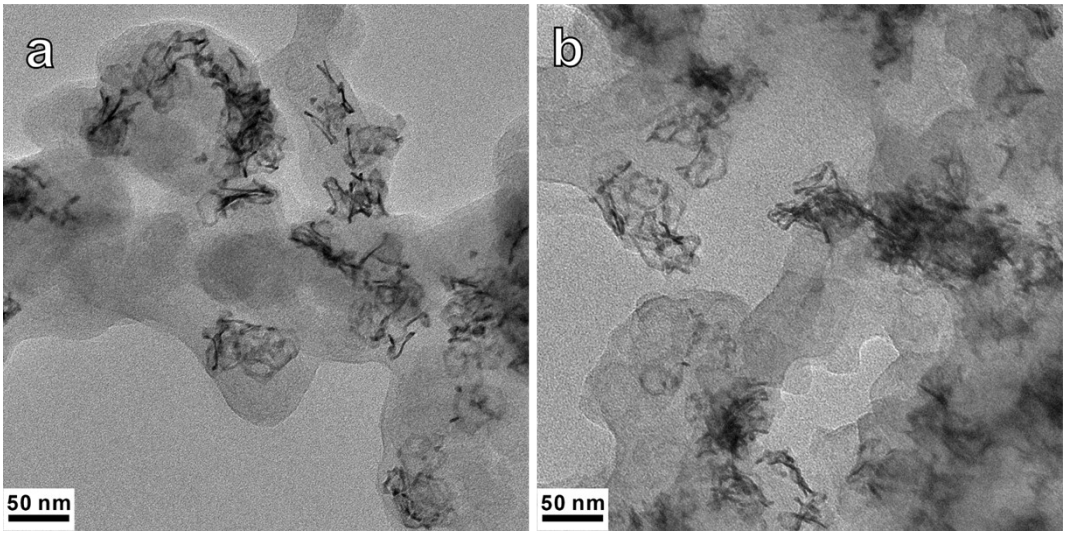

Fig. S11 TEM images of (**a**) initial $Pd_{45}Pt_{44}Ni_{11}$ SpNSs/C catalysts and (**b**) $Pd_{45}Pt_{44}Ni_{11}$ SpNSs/C catalysts after the 10 000-cycles ADT.

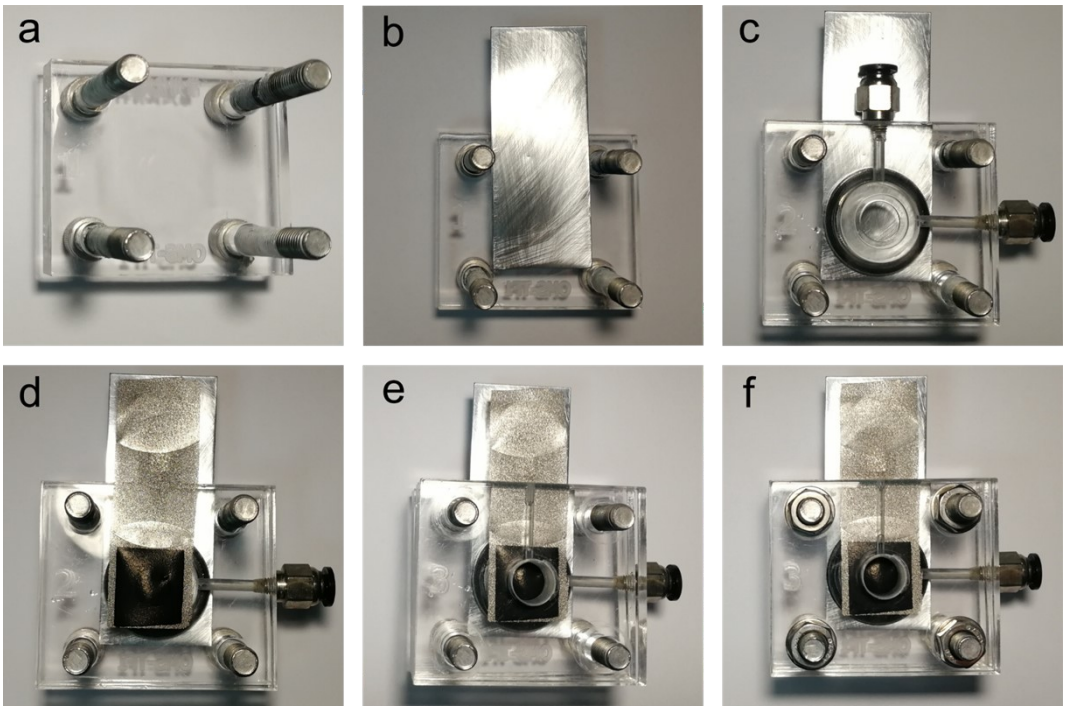

Fig. S12 Images showing the assembly sequence of the zinc-air battery in the order from a to f.

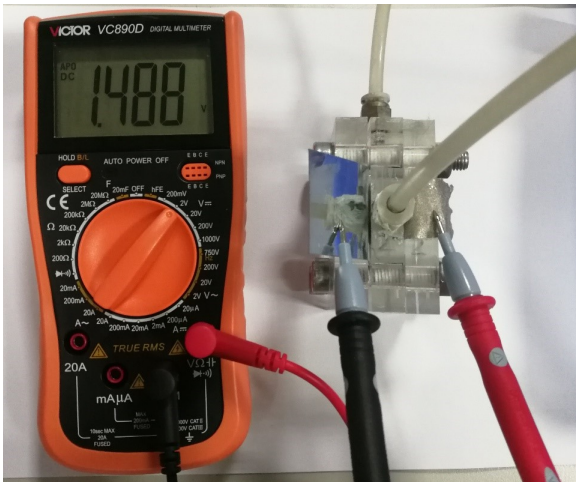

Fig. S13 The open-circuit voltage of $Pd_{45}Pt_{44}Ni_{11}$ SpNSs/C experimented in the Zn-air battery.

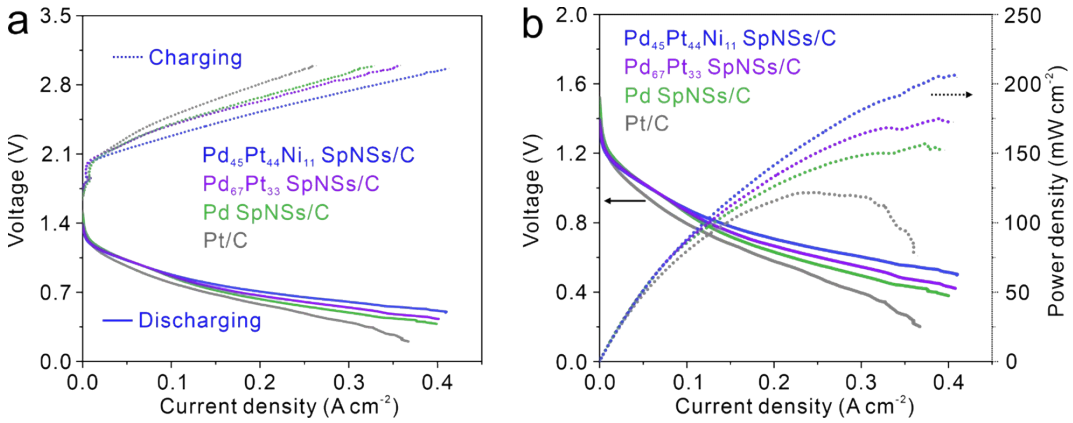

Fig. S14 (a) The charge and discharge performance and (b) power performance of the zinc-air battery of the $Pd_{45}Pt_{44}Ni_{11}$ SpNSs/C, $Pd_{67}Pt_{33}$ SpNSs /C, Pd SpNSs /C, and the commercial 20 wt% Pt/C.

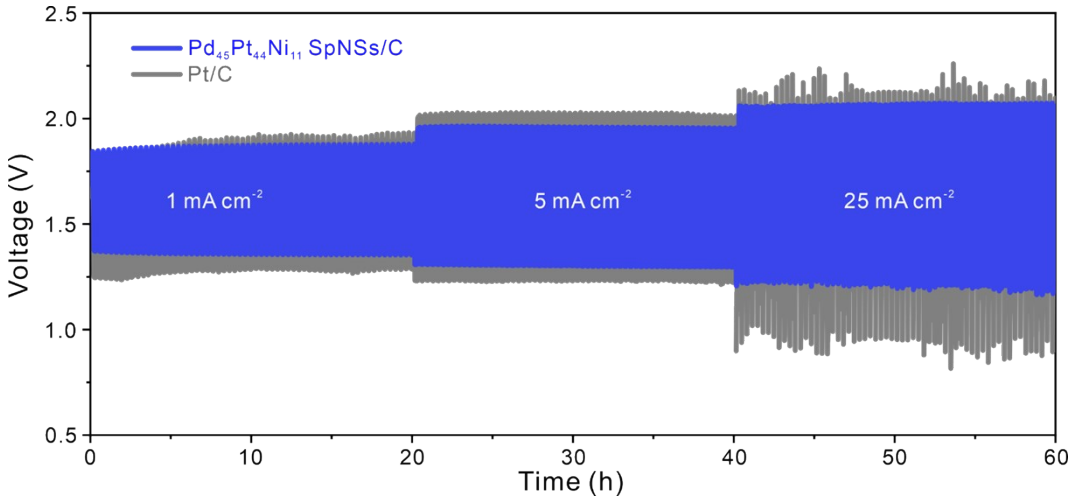

Fig. S15 Long-term cycling of the Zn-air batteries using $Pd_{45}Pt_{44}Ni_{11}$ SpNSs /C and Pt/C as the air electrode catalysts at different current densities.

Fig. S16 Photograph of a light board consisting of 37 LEDs illuminated by two Zn-air batteries in series.

Table S4. Performances of recently reported Pt- and Pd-based electrocatalysts in liquid Zn−air batteries.

Catalyst	Electrolyte	Peak power density [mW cm^{-2}]	Cycling current density [mA cm^{-2}]	Cycling stability	Reference
$Pd_{45}Pt_{44}Ni_{11}$ SpNSs	6 M KOH + 0.2 M Zinc acetate	206	10	220 h (660 cycles)	This work
CuPt-NC	6 M KOH	253.8	/	/	S1
O-PdFe@Pt/C	6 M KOH + 0.2 M Zinc acetate	342	5	126 h	S2
SA-PtCoF	6 M KOH + 0.2 M Zinc acetate	125	10	240 h	S3
ZIF-67@Pt/CB	6 M KOH + 0.2 M Zinc acetate	150	5	50 h	S4
Pd-Au/GO-4	6 M KOH	276	/	/	S5
PtFeNC-IrO_2	6 M KOH + 0.2 M Zinc acetate	148	10	24 h	S6
PdMo bimetallene/C	6 M KOH + 0.2 M Zinc acetate	154.2	10	350 cycles	S7
Pd/N–HsGY	6 M KOH	143	2	330 h	S8
$Pt_{1.1\%}Fe_{8.8\%}Ni$ PF	6 M KOH + 0.2 M Zinc acetate	175	20	500 h	S9
RuO_x-on-Pd NSs/C	6 M KOH + 0.2 M Zinc acetate	172	/	/	S10

References

S1. V. M. Dhavale and S. Kurungot, *ACS Catalysis*, 2015, **5**, 1445-1452.

S2. W. Xiao, M. A. L. Cordeiro, G. Gao, A. Zheng, J. Wang, W. Lei, M. Gong, R. Lin, E. Stavitski, H. L. Xin and D. Wang, *Nano Energy*, 2018, **50**, 70-78.

S3. Z. Li, W. Niu, Z. Yang, N. Zaman, W. Samarakoon, M. Wang, A. Kara, M. Lucero, M. V. Vyas, H. Cao, H. Zhou, G. E. Sterbinsky, Z. Feng, Y. Du and Y. Yang, *Energy Environ. Sci.*, 2020, **13**, 884-895.

S4. J. Li, Z. Meng, D. J. L. Brett, P. R. Shearing, N. T. Skipper, I. P. Parkin and S. Gadipelli, *ACS Appl. Mater. Interfaces*, 2020, **12**, 42696-42703.

S5. W. Zhu, H. Yuan, F. Liao, Y. Shen, H. Shi, Y. Shi, L. Xu, M. Ma and M. Shao, *Chemical Engineering Journal*, 2020, **389**, 124240.

S6. X. Zhong, S. Ye, J. Tang, Y. Zhu, D. Wu, M. Gu, H. Pan and B. Xu, *Applied Catalysis B: Environmental*, 2021, **286**, 119891.

S7. M. Luo, Z. Zhao, Y. Zhang, Y. Sun, Y. Xing, F. Lv, Y. Yang, X. Zhang, S. Hwang, Y. Qin, J.-Y. Ma, F. Lin, D. Su, G. Lu and S. Guo, *Nature*, 2019, **574**, 81-85.

S8. W. Si, Z. Yang, X. Hu, Q. Lv, X. Li, F. Zhao, J. He and C. Huang, *Journal of Materials Chemistry A*, 2021, **9**, 14507-14514.

S9. G. Wang, J. Chang, S. Koul, A. Kushima and Y. Yang, *J. Am. Chem. Soc.*, 2021, **143**, 11595-11601.

S10. Z. Lyu, X.-G. Zhang, Y. Wang, K. Liu, C. Qiu, X. Liao, W. Yang, Z. Xie and S. Xie, *Angew. Chem. Int. Ed.*, 2021, **60**, 16093-16100.